

Structural Basis for Recognition of Diubiquitins by NEMO

Yu-Chih Lo,¹ Su-Chang Lin,¹ Carla C. Rospigliosi,¹ Dietrich B. Conze,² Chuan-Jin Wu,² Jonathan D. Ashwell,² David Eliezer,¹ and Hao Wu^{1,*}

¹Department of Biochemistry, Weill Cornell Medical College, New York, NY 10021, USA

²Laboratory of Immune Cell Biology, Center for Cancer Research, National Cancer Institute, National Institutes of Health, Bethesda, MD 20892, USA

*Correspondence: haowu@med.cornell.edu

DOI 10.1016/j.molcel.2009.01.012

SUMMARY

NEMO is the regulatory subunit of the I κ B kinase (IKK) in NF- κ B activation, and its CC2-LZ region interacts with Lys63 (K63)-linked polyubiquitin to recruit IKK to receptor signaling complexes. In vitro, CC2-LZ also interacts with tandem diubiquitin. Here we report the crystal structure of CC2-LZ with two dimeric coiled coils representing CC2 and LZ, respectively. Surprisingly, mutagenesis and nuclear magnetic resonance experiments reveal that the binding sites for diubiquitins at LZ are composites of both chains and that each ubiquitin in diubiquitins interacts with symmetrical NEMO asymmetrically. For tandem diubiquitin, the first ubiquitin uses the conserved hydrophobic patch and the C-terminal tail, while the second ubiquitin uses an adjacent surface patch. For K63-linked diubiquitin, the proximal ubiquitin uses its conserved hydrophobic patch, while the distal ubiquitin mostly employs the C-terminal arm including the K63 linkage residue. These studies uncover the energetics and geometry for mutual recognition of NEMO and diubiquitins.

INTRODUCTION

NF- κ B proteins are evolutionarily conserved master regulators of immune and inflammatory responses (Gilmore, 2006). They play critical roles in a wide array of biological processes, including innate and adaptive immunity, oncogenesis, and development. They are activated in response to ligation of many receptors, including T cell receptors, B cell receptors, and members of the tumor necrosis factor (TNF) receptor superfamily and the Toll-like receptor/interleukin-1 receptor (TLR/IL-1R) superfamily. The Ser/Thr-specific I κ B kinase (IKK) signalosome is at the bottleneck for NF- κ B activation because activated IKK phosphorylates I κ B, leading to Lys48 (K48)-linked polyubiquitination and subsequent degradation of I κ B by the proteasome (Scheidereit, 2006). The freed NF- κ B dimers translocate to the nucleus to mediate specific target gene transcription.

The IKK signalosome contains the kinase, IKK α and/or IKK β , and the highly conserved regulatory protein NEMO (also known as IKK γ or FIP-3) (Scheidereit, 2006). IKK activity relies on the interaction between the kinase and NEMO. In cells lacking NEMO, IKK α and IKK β cannot be activated by any of the classical NF- κ B inducers. Sequence analysis of NEMO indicates a high helical content with an N-terminal kinase-binding domain (KBD), three coiled-coil regions (CC1, CC2, and LZ) and a zinc-finger (ZF) domain (Scheidereit, 2006).

IKK activation by multiple receptor signaling pathways has been shown to depend on Lys63 (K63)-linked nondegradative polyubiquitination (Chen, 2005). For the IL-1 and the Toll-like receptor signaling pathways, the RING domain ubiquitin (Ub) ligase (E3) TRAF6, in conjunction with the specific dimeric Ub-conjugating enzyme Ubc13/Uev1A complex (E2), is responsible for K63-linked polyubiquitination of itself and downstream proteins such as IRAK1. For the TNF α signaling pathway, the RIP1 kinase is K63 polyubiquitinated (Ea et al., 2006; Wu et al., 2006). Similarly, K63-linked polyubiquitination of T cell signaling mediators MALT1 (Oeckinghaus et al., 2007) and Bcl10 (Wu and Ashwell, 2008) is critical for NF- κ B activation.

Recent studies have shown that direct binding of NEMO to K63-linked polyubiquitin (poly-Ub) chains is crucial for IKK recruitment and NF- κ B activation (Ea et al., 2006; Wu et al., 2006). A yeast two-hybrid screen pulled out tandem diubiquitin (di-Ub) or triubiquitin (tri-Ub) molecules, which are endogenous Ub precursors, as NEMO-interacting proteins (Wu et al., 2006). NEMO interacted with K63-polyubiquitinated RIP1 in the TNF α signaling pathway (Ea et al., 2006) and bound K63-linked poly-Ub in vitro (Ea et al., 2006; Wu et al., 2006). Presumably, the K63-linked poly-Ub chains serve as an extended scaffold for signal-dependent NEMO recruitment and oligomerization.

Deletion mapping experiments revealed that the region encompassing the CC2 and LZ domains was necessary and sufficient for Ub interaction (Ea et al., 2006; Wu et al., 2006). The interaction required a minimum of di-Ub, and little interaction could be detected with monoubiquitin (mono-Ub). A region of high homology with NEMO within the CC2-LZ region has been identified in the NEMO-like proteins Optneurin and ABIN1-3 and was named the UBAN domain (Wagner et al., 2008). Interestingly, naturally occurring point mutations of NEMO in this region have been shown to impair NF- κ B activation and cause a diverse array of serious X-linked diseases such as ectodermal dysplasia and immunodeficiency in human patients (Courtois and Gilmore,

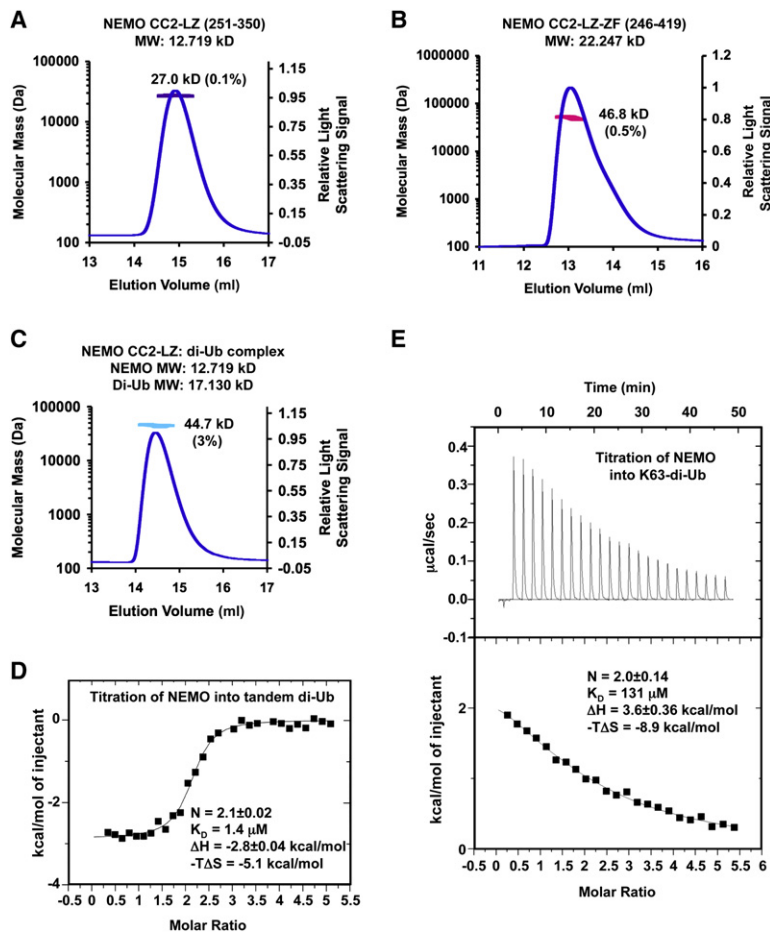


Figure 1. CC2-LZ of NEMO Is Dimeric and Interacts with Di-Ub at 2:1 Stoichiometry

(A) Multiangle light scattering (MALS) measurement of NEMO CC2-LZ (residues 251–350), showing the relative light scattering signal as a function of elution volume. The derived molecular mass of the peak is shown in violet, which matches the reading on the left axis.

(B) MALS measurement of NEMO CC2-LZ-ZF (residues 246–419). The derived molecular mass of the peak is shown in pink.

(C) MALS measurement of the complex of NEMO CC2-LZ (residues 251–350) and tandem di-Ub. The derived molecular mass of the peak is shown in cyan.

(D) Isothermal titration calorimetry (ITC) measurement of the NEMO:tandem di-Ub interaction. NEMO was titrated into the tandem di-Ub solution. The numbers show the fitting of the data, with N for stoichiometry, K_D for dissociation constant, ΔH for enthalpy change, and $-\Delta S$ for entropy change.

(E) ITC measurement of the NEMO:K63-di-Ub interaction. NEMO was titrated into the K63-di-Ub solution.

2006; Filipe-Santos et al., 2006; Sebban-Benin et al., 2007). The immunological, skin and hair features observed in these patients may result from defective responses to many extracellular and cell surface ligands such as EDA, LPS, IL-1, IL-18, TNF α , TLR2, and CD40L.

The molecular mechanism of di-Ub recognition by NEMO is entirely unknown. Here, we report the crystal structure of the CC2-LZ region of NEMO, which revealed an elongated dimeric molecule with two coiled coils and an intervening bend. Because of the ability of the CC2-LZ region to interact with both tandem and K63-linked di-Ub, we used the former as a reasonable starting point to address NEMO:K63-linked di-Ub interaction. The N terminus and the K63 side chain of Ub are spatially proximal so that tandem and K63-linked di-Ub may have similar structural properties in NEMO interaction. To map the mutual binding sites of NEMO with tandem and K63-linked di-Ub, we used a combination of structure-based mutagenesis and nuclear magnetic resonance (NMR). Surprisingly, the binding site of NEMO for tandem and K63-linked di-Ub, which is localized to the LZ coiled coil, is a composite of both chains of the NEMO dimer, unlike known helical motifs involved in Ub interactions (Hurley et al., 2006). This Ub-binding site of NEMO explains many NEMO disease-causing mutations. Our mutagenesis data on individual Ub molecules within tandem di-Ub and K63-linked di-Ub and NMR chemical shift perturbation data using selectively labeled

di-Ub showed both similarities and differences in the modes of these NEMO:di-Ub interactions. The mapped mutual interaction surfaces allowed information-restrained docking to generate both NEMO:tandem di-Ub and NEMO:K63-linked di-Ub models. For tandem di-Ub, the conserved hydrophobic patch of the first Ub and an adjacent and overlapping surface patch of the second Ub clasp around NEMO. For K63-linked di-Ub, the conserved hydrophobic patch of the proximal Ub contributes more to the overall NEMO interaction than that of the distal Ub, and the C-terminal tails of both proximal and distal Ub are involved in

NEMO interaction. Collectively, these studies provided mechanistic insight into the mutual recognition of NEMO and di-Ub.

RESULTS

The CC2-LZ Region Is Dimeric, and Each CC2-LZ Dimer Interacts with One Tandem or K63-Linked Di-Ub

As a first step toward understanding the interaction of NEMO with poly-Ub, we expressed and purified the putative Ub-binding domain comprising the CC2-LZ region of human NEMO (residues 251–350). Gel filtration analysis showed a homogeneous size distribution of CC2-LZ. The oligomerization state could not be determined because the coiled-coil structure of the region is likely to be nonglobular. To accurately determine the native molecular mass of CC2-LZ, we used multiangle light scattering (MALS) in conjunction with refractive index, which measures molecular mass independent of its molecular shape. The measurement revealed a homogeneous species for CC2-LZ with a molecular mass of 27.0 kD (0.1% error). Because the calculated molecular weight of the CC2-LZ construct is 12.719 kD, this measurement is consistent with a dimeric structure of CC2-LZ (Figure 1A). Similarly, MALS measurement of the entire C-terminal region of NEMO comprising CC2, LZ, and ZF domains (residues 246–419) also revealed a homogeneous dimer (Figure 1B). This is in contrast to the previously suggested

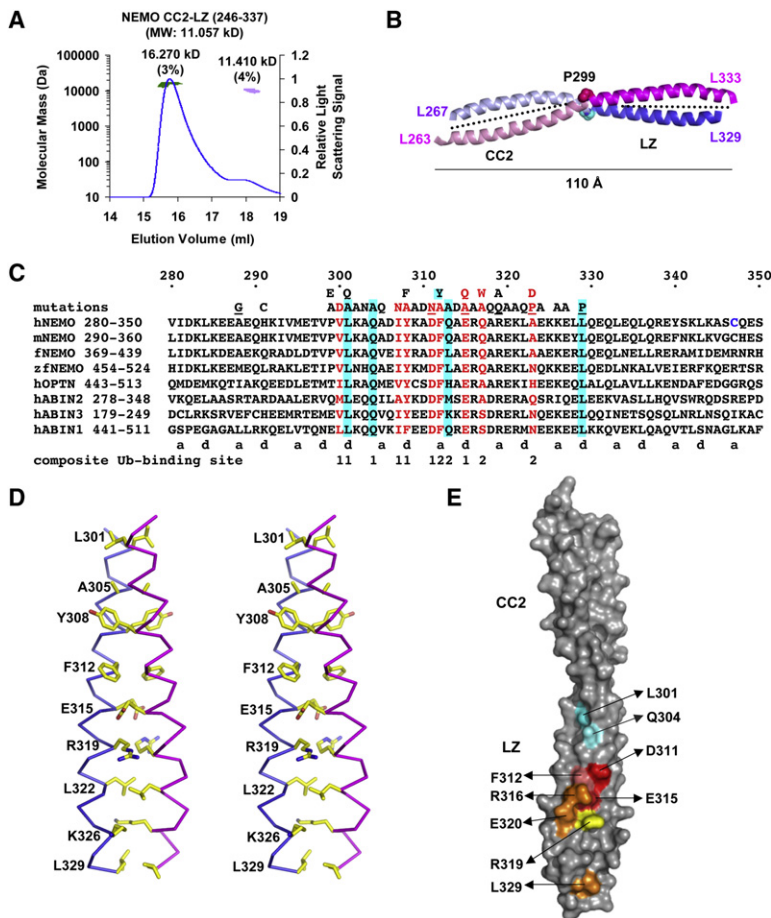


Figure 2. Structure of CC2-LZ

(A) MALS measurement of NEMO CC2-LZ (residues 246–337). The major peak (shown in green) corresponds to monomer-dimer equilibrium.

(B) Overall structure of CC2-LZ. The N- and C-terminal residues and P299 are labeled. Approximate 2-fold axes of the coiled coils are shown by dotted lines. There is a 20° kink between the CC2 and the LZ coiled coils. The overall dimension of the structure is shown.

(C) Sequence alignment of CC2-LZ from different species of NEMO and from ABIN1-3 and Optineurin. Mutations of NEMO are shown above the sequence: red, cyan, and black indicate drastic, weak, and no effects, respectively. Two slight differences between tandem and K63-linked di-Ub were observed. While R319Q had a weak effect on tandem di-Ub interaction, it had no effect on K63-di-Ub interaction. L329P had no effect on tandem di-Ub interaction but had a weak effect on K63-di-Ub interaction. Known disease mutations of NEMO are underlined. C347 is shown in blue. The a and d positions in the coiled coils are labeled below the sequence. Residues important for Ub binding are labeled “1” or “2” depending on which chain they come from in the composite Ub-binding site. Part of the sequence of CC2 is omitted in this alignment because there are no absolutely conserved residues in that region. h, human; m, mouse; f, frog; zf, zebrafish.

(D) Stereo diagram of the LZ region showing the side chains at the a and d positions of the coiled coil.

(E) Mapping of strictly conserved residues onto the CC2-LZ structure. Each residue is shown with a distinct color that matches the colors for mutational effects in Figure 4.

trimeric architecture of the CC2-LZ region of mouse NEMO for which the equilibrium ultracentrifugation experiment performed in the presence of the detergent n-dodecyl-β-d-maltopyranoside (DDM) showed equilibrium between monomer, dimer, and trimer (Agou et al., 2002).

Consistent with previous data (Ea et al., 2006; Wu et al., 2006), the CC2-LZ construct interacted with tandem di-Ub or K63-linked di-Ub as shown by pull-down experiments using His-tagged NEMO (see below). Using gel filtration coupled with MALS, we showed that each CC2-LZ dimer forms a stoichiometric complex with one tandem di-Ub (Figure 1C). The measured molecular mass of the complex is 44.7 kD, while the calculated molecular weight for two CC2-LZ and one di-Ub is 42.6 kD. We further measured the binding affinity of CC2-LZ with mono-Ub, tandem di-Ub, and K63-linked di-Ub quantitatively using isothermal titration calorimetry (ITC). No interaction could be detected between NEMO and mono-Ub, while dissociation constants of 1.4 μM and 131 μM were obtained for the NEMO:tandem di-Ub and the NEMO:K63-linked di-Ub interactions, respectively (Figures 1D and 1E). The measured stoichiometries for the titration of NEMO into tandem and K63-linked di-Ub were 2.1 ± 0.02 and 2.0 ± 0.14, respectively, demonstrating that each di-Ub interacts with one NEMO dimer. The fairly low affinity of NEMO to K63-linked di-Ub suggests that longer chain of K63-linked poly-Ub may be required for its inter-

action with NEMO in cells (Wu et al., 2006), likely through higher-order oligomerization of NEMO.

Crystal Structure of CC2-LZ

We crystallized a shorter version of the CC2-LZ region of NEMO (residues 246–337). This region exists in monomer-dimer equilibrium in solution as shown by MALS (Figure 2A) but forms a dimeric coiled coil in the crystal (Figure 2B). The structure was initially determined at 4.0 Å resolution using single-wavelength anomalous diffraction on a selenomethionyl crystal (Se-SAD) (Table 1). The solvent content of the crystal is approximately 73%. Although the electron density map revealed the overall shape of the structure, it was not of sufficient quality for sequence fitting. To enhance anomalous signal and improve phasing, we generated mutations to Met on several conserved hydrophobic residues at the predicted a or d positions of the CC2-LZ and were able to obtain a 3.2 Å resolution Se-SAD data set on the L263M/L267M double mutant (Table 1). Similar to the wild-type (WT) protein, the mutant efficiently pulled down tandem and K63-linked di-Ub (data not shown). The resulting electron density map was of sufficient quality to allow model building and refinement. The structure contains ordered residues 263–333 for one chain and residues 267–329 for the other chain.

The structure revealed an elongated dimer of CC2-LZ that spans approximately 110 Å (Figure 2B). Based on the secondary

Table 1. Crystallographic Statistics

	NEMO	NEMO (L263M/L267M)
Constructs	residues 246–337	residues 246–337
Structure determination	SAD	SAD
Data collection		
Beamlines	NE-CAT ID-C of APS	NE-CAT ID-C of APS
Space group	P6 ₅	P6 ₅
Cell dimensions, a, b, c	77.8 Å, 77.8 Å, 77.1 Å	76.2 Å, 76.2 Å, 76.9 Å
Resolution	50–4.0 Å	35–3.2 Å
R _{sym}	5.2% (44.4%)	5.8% (54.6%)
I/σI	12.7 (4.3)	11.3 (2.4)
Completeness	99.7% (99.7%)	99.0% (99.4%)
Redundancy	5.5 (5.5)	5.4 (5.6)
Refinement		
Resolution		30–3.2 Å
No. reflections		4105
R _{work} /R _{free}		24.5%/30.7%
No. protein atoms		1089
R.m.s. deviations		
Bond lengths/angles		0.007 Å/1.39°
Ramachandran plot		
Most favored/allowed		90.0%/10.0%

Highest-resolution shell is shown in parenthesis.

structure definition in Procheck, each chain of the CC2-LZ dimer forms a continuous helix. However, there is a prominent kink of about 20° near residue P299, which may be used as the boundary between the CC2 coiled coil and the LZ coiled coil. This boundary is somewhat different from the previous definition of the CC2 and LZ region based on sequence analyses (Scheidereit, 2006). The full CC2-LZ structure does not have 2-fold symmetry. When the two chains of CC2 are structurally aligned, the LZ chains are not superimposed and vice versa. However, the individual CC2 and LZ coiled coils almost obey 2-fold symmetry, with CC2 having 179° rotation and LZ having 171° rotation between the two chains. The a and d positions of both CC2 and LZ are often noncanonical dimeric coiled-coil residues including charged residues (Figure 2C), perhaps explaining the apparent weak dimerization of the CC2-LZ construct (residues 246–337). At the dimerization interface, the hydrophobic portions of these residues pack against each other with their hydrophilic portions facing outwards (Figure 2D). It has been shown that NEMO forms intermolecular disulfide bonds through C54 and C347 (Herscovitch et al., 2008). C347 is within the longer CC2-LZ construct (residues 251–350), which may stabilize dimerization via the intermolecular disulfide bond.

Mapping of residues in the CC2-LZ region that are conserved among NEMO, Optineurin, and ABIN1-3 onto the structure revealed two symmetrical surface patches at the LZ region (Figures 2C and 2E). In contrast, the CC2 region does not contain any strictly conserved residues. Interestingly, the conserved

surface patches are formed compositely from both chains of the dimeric coiled coil. They each include residues L301, Q304, D311, and E315 from one chain and F312, R316, R319, E320, and L329 from the other chain. The surface conservation pattern clearly suggests that the LZ region harbors the Ub-binding site of NEMO. The LZ region coincides with the UBAN domain common to NEMO, Optineurin, and ABIN1-3 (Wagner et al., 2008).

Identification of a Composite Ub-Binding Site that Is Completely Different from the UIM/MIU Motif

Because repeated attempts to crystallize CC2-LZ in complex with di-Ub failed to yield any useful crystals, we first used the mutagenesis approach to map the tandem di-Ub binding site in NEMO (Figures 2C and 3A). Mutational effects were assessed by pull-down experiments using His-tagged WT and mutant CC2-LZ of NEMO (residues 251–350) and nontagged tandem di-Ub. The mutagenesis went through several stages. First, we mutated all conserved residues in the LZ/UBAN domain. Second, we mutated all Ala residues and additional hydrophobic residues in LZ, because we wondered whether NEMO interacts with Ub via a “cryptic” helical UIM or MIU motif, for which the consensus sequence includes an absolutely conserved Ala residue and several hydrophobic residues (Hurley et al., 2006). Third, we mutated all known NEMO disease mutations in the LZ region. Fourth, we produced conserved substitutions on the highly defective mutations. We found that even conserved mutations D311N, E315Q, and F312Y are severely or partially defective in di-Ub binding, suggesting that the charges and the exact fit of the side chains are crucial for di-Ub interaction. Eventually, we generated structure-based mutations on almost all residues in the conserved LZ region. Collectively among the 38 mutations, V300D, I307N, Y308A, D311N, F312A, E315A/Q, Q317A/W, and A323P/D nearly abolished the ability of NEMO to interact with tandem di-Ub (Figures 2C and 3A). L301A, Q304A, F312Y, Q313A, and R319Q significantly decreased tandem di-Ub binding (Figures 2C and 3A).

To determine whether NEMO residues important for tandem di-Ub interaction are also critical for K63-linked di-Ub interaction, we enzymatically synthesized K63-linked di-Ub for use in pull-down by His-tagged NEMO (Piotrowski et al., 1997). We generated two Ub mutant constructs: K63R-Ub and D77-Ub, in which a D77 residue is appended to the last residue G76 of Ub. In a ubiquitination assay with E1 and the E2 complex Ubc13/Uev1A, these two Ub mutants together generate only K63-linked di-Ub, with K63R-Ub as the distal Ub and D77-Ub as the proximal Ub (Piotrowski et al., 1997). When tested for binding to K63-linked di-Ub, all but one of the NEMO mutations had effects similar to tandem di-Ub (Figure 3B and Figure S1 [available online]). R319Q is significantly defective in binding to tandem di-Ub but appears to be WT in binding to K63-linked di-Ub. In general, these data confirm that tandem di-Ub is a good mimic for K63-linked di-Ub, but there may be subtle differences in their binding to NEMO.

To determine whether these mutations defective in tandem and K63-linked di-Ub binding also caused global disruption of the dimeric coiled-coil structure, we utilized the ability of the WT CC2-LZ construct to form an intermolecular disulfide bond

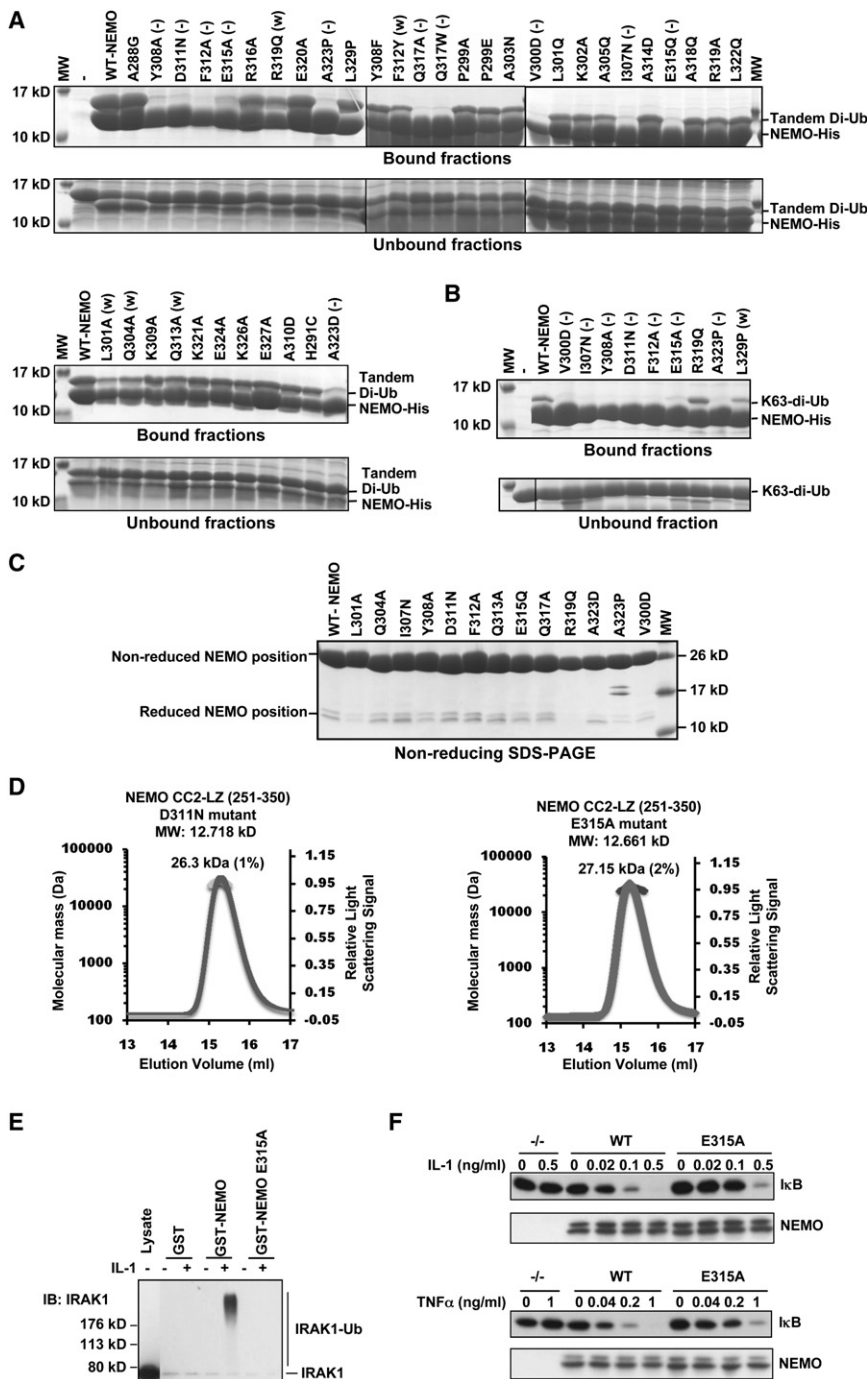


Figure 3. Structure-Based Mutagenesis of NEMO

(A) Pull-down of nontagged tandem di-Ub by WT and mutant CC2-LZ (residues 251–350). –, essentially no binding; w, weak binding. (B) Pull-down of K63-linked di-Ub by WT and mutant CC2-LZ (residues 251–350). –, essentially no binding; w, weak binding. (C) Nonreducing SDS-PAGE of CC2-LZ mutants that are defective in di-Ub interaction, showing their dimeric state. (D) MALS measurements of selective CC2-LZ mutants, showing their dimeric state. (E) The E315A mutant is defective in interacting with K63-polyubiquitinated IRAK1 in IL-1 signaling. Cell lysates from 293 cells stably expressing IL-1R that had been stimulated with or without IL-1 (10 ng/ml) for 5 min were incubated with GST, GST-NEMO, or GST-NEMO E315A mutant-coated beads, and the bead-bound complexes were immunoblotted (IB) with anti-IRAK-1. (F) The E315A mutant is defective in rescuing NEMO-deficient cells in IL-1 and TNF α -induced I κ B degradation. Cell lysates from NEMO-deficient MEFs or NEMO-deficient cells stably expressing HA-tagged NEMO (WT) or HA-tagged NEMO E315A mutant that had been stimulated with the indicated amounts of IL-1 or TNF α for 10 min were immunoblotted with anti-I κ B and anti-NEMO.

of the dimeric nature of these mutants came from measurements by MALS (Figures 3D and S2). Therefore, these mutants do not appear to have destroyed the global conformation of the dimeric coiled coil.

Mapping of residues important for tandem and K63-linked di-Ub interaction onto the CC2-LZ structure showed that they form symmetrical composite Ub-binding sites (Figure 4). Each surface patch is formed from both chains, V300, L301, Q304, I307, Y308, D311, and E315 from one chain, and F312, Q313, Q317, and A323 from the other chain (Figure 4A). A mixture of hydrophobic and hydrophilic components is present at the mapped Ub-binding site (Figures 4B and 4C). These residues are highly

conserved, but not always identical in Optineurin and ABIN1-3, suggesting a similar, but not identical mode of Ub-binding in these NEMO-related proteins (Figure 2C). The two symmetrical surface patches of NEMO are clearly separated by residues at the sides that do not participate in Ub binding (Figure 4B). The composite nature of the mapped Ub-binding site distinguishes itself from many helical motifs in Ub recognition, such as the UIM and MIU, in which a single helix contributes all the interactions (Hurley et al., 2006).

at C347. In the absence of the reducing agent dithiothreitol (DTT), WT CC2-LZ migrated at the dimeric molecular weight on an SDS-PAGE (Figure 3C). Upon treatment with DTT, WT CC2-LZ migrated at the monomeric molecular weight (Figure 3A). We reasoned that if the mutations drastically destabilized the dimeric coiled coil, the disulfide bond would fail to form. All mutants that are defective in di-Ub binding showed the presence of the disulfide bonds, suggesting that the dimeric coiled coils were formed in these mutants (Figure 3C). Further confirmation

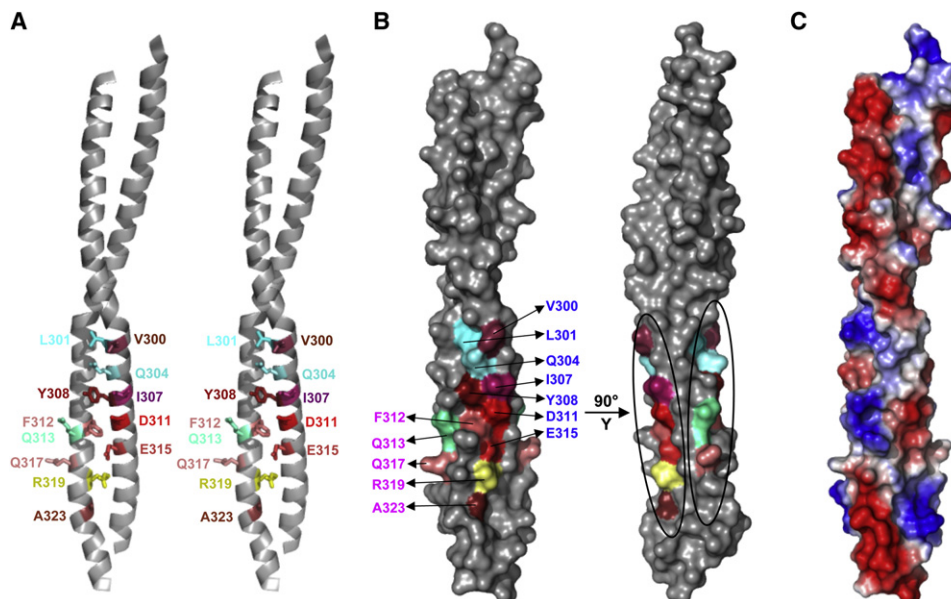


Figure 4. Mapped Ub-Binding Site of NEMO

(A) NEMO residues that are important for tandem and K63-linked di-Ub interaction are shown in the stereo ribbon diagram of the CC2-LZ structure. Residues labeled in the red shades caused most drastic effects when mutated. Those labeled in the cyan shades caused less drastic effects. R319 is shown in yellow to indicate that it is involved in tandem, but not K63-linked, di-Ub binding.

(B) The same residues are shown on a surface representation of the structure. Residues from one chain are labeled on the left, and residues from the other chain are labeled on the right of the structure. The ovals at the right panel indicate the two separate symmetrical Ub-binding sites.

(C) The electrostatic surface representation of CC2-LZ.

The Mapped Di-Ub-Binding Site of NEMO Is Important for NF- κ B Activation

To determine whether the Ub-binding site of NEMO identified using *in vitro* biochemical assay is important for its cellular function, we picked a crucial residue E315 for functional assessment. E315A and E315Q mutations are severely defective in interactions with tandem and K63-linked di-Ub. E315A is also a naturally occurring disease-causing mutation (Filipe-Santos et al., 2006). 293 cells stably expressing the IL-1 receptor were stimulated or not with IL-1 and lysed. GST or the indicated NEMO GST-fusion proteins were used to pull down IRAK-1 in the cell lysates (Figure 3E). Whereas none of the constructs pulled down IRAK-1 in unstimulated cells, WT NEMO brought down ubiquitinated (but not unmodified) IRAK-1 from IL-1 stimulated cells. In contrast, the E315A mutant did not bring down IRAK-1 under these conditions.

To further explore the effect of the E315A mutation on physiologic signals leading to NF- κ B activation, we stably expressed WT NEMO or its E315A mutant in NEMO-deficient murine embryonic fibroblasts (MEFs), and clones that expressed similar amounts of NEMO were selected for study. Degradation of I κ B was used as a sensitive and specific indicator of IKK activity. Stimulation of the NEMO-deficient MEFs with either IL-1 (Figure 3F, top panel) or TNF α (Figure 3F, lower panel) did not cause I κ B degradation. In contrast, I κ B degradation was observed in MEFs reconstituted with WT NEMO upon stimulation with either IL-1 or TNF α in a dose-responsive fashion. Cells reconstituted with the E315A mutant also degraded I κ B but were much less sensitive to these cytokines. For example, 5- to 10-fold more IL-1 and 5-fold more TNF α were required to achieve the same

degree of I κ B degradation in cells expressing mutant NEMO as in those expressing WT NEMO. These data are representative of two (WT NEMO) and three (E315A NEMO) independent clones. Therefore, the E315A mutation impaired NEMO binding to ubiquitinated signaling intermediates and reduced the efficiency of receptor-mediated signaling for IKK activity. Defective di-Ub interactions *in vitro* for mutations of Y308 and F312 are consistent with previous results showing the failure of these mutant forms of NEMO to be activated by TRAF6 and mediate TNF α -induced NF- κ B activation (Ea et al., 2006). Collectively, these data link *in vitro* poly-Ub binding to signal-dependent NF- κ B activation in cells.

The Structure Explains NEMO Disease-Causing Mutations

NEMO is located on the X chromosome, and many of its mutations have been associated with distinct X-linked genetic diseases. At least five point mutations in the CC2-LZ region have been shown to cause NEMO dysfunction. The A288G, D311N, and A323P (Courtois and Gilmore, 2006; Sebban-Benin et al., 2007) mutations cause severe anhidrotic ectodermal dysplasia with immunodeficiency (EDA-ID), in which the patients suffer skin inflammation and impaired NF- κ B activation in response to numerous stimuli such as TNF α , IL-1, and LPS. The E315A and R319Q mutations were identified as immunodeficiency against mycobacterial infections and caused impairment in IL-12 production (Filipe-Santos et al., 2006).

Our structure provides a mechanistic basis for some of these NEMO mutations. D311N and E315A most likely disrupt di-Ub

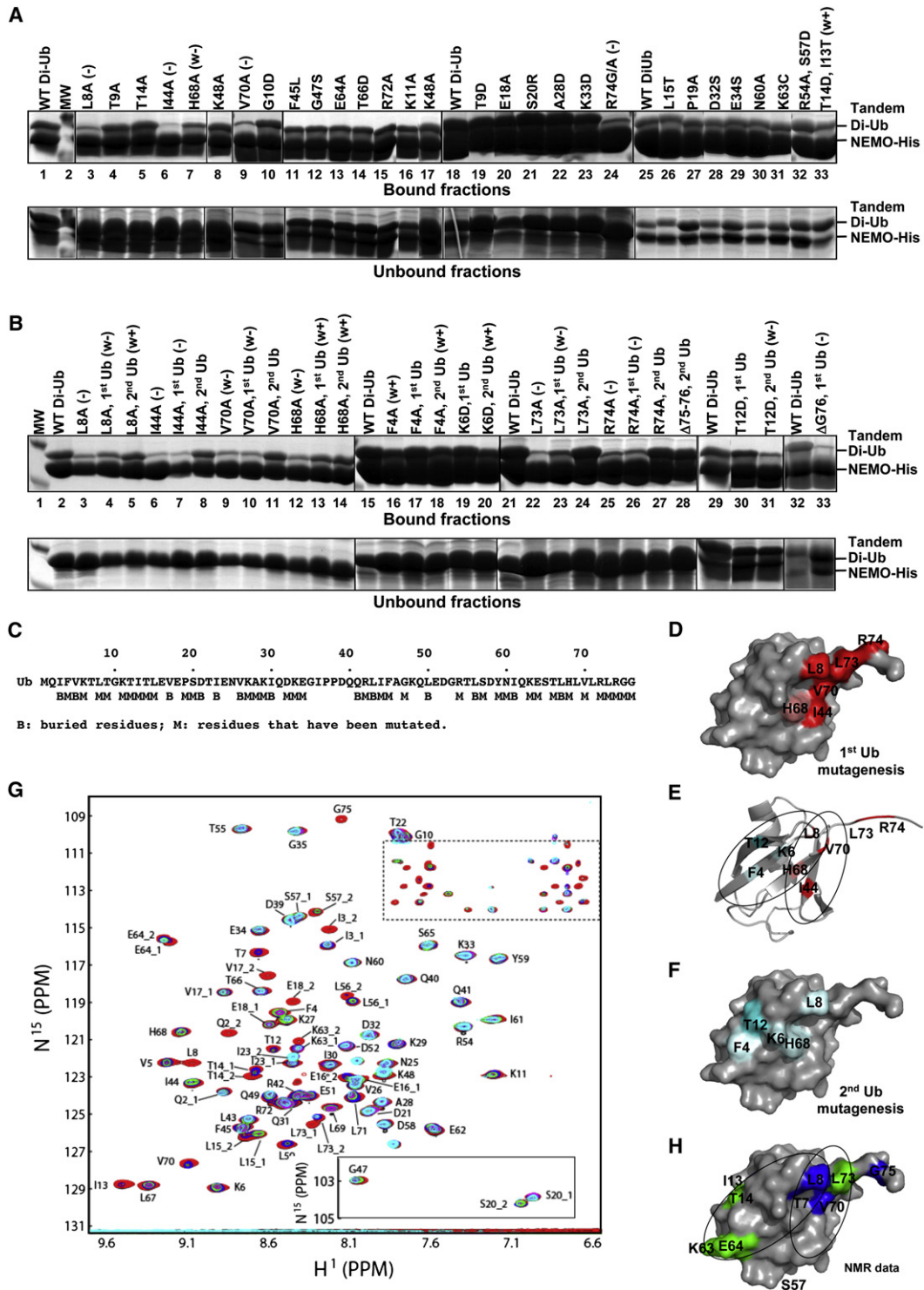


Figure 5. Structure-Based Mutagenesis and NMR Experiments on the NEMO:Tandem Di-Ub Interaction

(A) Mutations on tandem di-Ub. Both Ub molecules are mutated except when noted. R74G/A means R74G in the first Ub and R74A in the second Ub of the tandem di-Ub. The bound di-Ub amounts were semiquantified. No effects, >0.8 of WT; w+, 0.5–0.8 of WT; w–, 0.2–0.5 of WT; –, <0.2 of WT.

(B) Mutations on either the first or the second Ub of the tandem di-Ub. No effects, >0.8 of WT; w+, 0.5–0.8 of WT; w–, 0.2–0.5 of WT; –, <0.2 of WT.

(C) Summary of the Ub residues that have been mutated.

(D) Mapping of mutational data onto the first Ub surface of the tandem di-Ub. Red, drastic effects; pink, less drastic effects.

binding via a direct loss of binding energy, as they reside within the core portion of the mapped Ub-binding site (Figures 4A and 4B). For E315A, we showed that it compromised signal-dependent NF- κ B activation (Figure 3F). One would have predicted that the A323P mutation could distort the local coiled-coil structure of the LZ domain, but the A323D mutation is also defective in di-Ub binding. This suggests that A323 may directly contact Ub. Lack of global conformational disturbances of these mutations is confirmed by MALS and their ability to form disulfide-linked dimers (Figures 3C and 3D).

The A288 G mutation did not cause any effect on di-Ub interaction. In addition, the mutant was able to form disulfide-linked dimers, precluding dramatic conformational changes. Since A288 is also quite far away from the mapped Ub-binding site, our data are consistent with the previous explanation that the mutant may have reduced temperature-dependent oligomer stability (Vinolo et al., 2006). Since R319Q did not show observable defects in K63-linked di-Ub interaction, the molecular basis of this disease mutation may be related to other aspects of NEMO function or its expression level and stability in vivo.

The Conserved Hydrophobic Surface of Ub near I44 in Tandem Di-Ub Is a Major NEMO-Binding Site

To elucidate the structural determinant on Ub for NEMO interaction, we first generated site-directed mutations on both Ub molecules of tandem di-Ub. The importance of hydrophobic residues of NEMO, especially near the center of the mapped Ub-binding site, prompted us to investigate the role of the hydrophobic patch of Ub near residue I44, which is a hot spot for protein interactions (Hurley et al., 2006). Mutations were also made of residues that exhibited chemical shift perturbations upon titration of ABIN-1 into mono-Ub (Wagner et al., 2008). Additional mutations were designed to cover a majority of the exposed surface of Ub.

The mutagenesis identified L8, I44, and V70 as crucial Ub residues for NEMO interaction because L8A, I44A, and V70A mutations at both Ub molecules in the tandem di-Ub nearly abolished interactions with NEMO (Figure 5A, lanes 3, 6, and 9). H68A decreased but not abolished NEMO interaction (lane 7). Residue R74, which resides on the C-terminal tail of Ub, was also identified as critical for NEMO interaction (lane 24). Its importance may be consistent with the absolute requirement of acidic residues D311 and E315 of NEMO in their mutual interaction and may indicate the involvement of the linkage between the first and second Ub. In contrast, the remaining 24 mutations did not have apparent effects on NEMO binding. These data demonstrate that tandem di-Ub uses the conserved hydrophobic patch on the face of its five-stranded β sheet for NEMO interaction. This

same surface patch is typically recognized by other ubiquitin binding domains as well (Hurley et al., 2006).

Mutagenesis and NMR Studies Identified Two Overlapping NEMO-Binding Sites on the First and Second Ub of Tandem Di-Ub

To determine whether the two Ub molecules of tandem di-Ub interact similarly with NEMO, we generated L8A, I44A, V70A, and H68A mutations on either the first or second Ub molecules and compared their effects on NEMO interaction (Figures 5B and 5C). Strikingly, the I44A and V70A mutations in the first Ub had as strong effects on NEMO binding as the mutations on both Ub molecules, while the same mutations in the second Ub had no effects on NEMO binding (Figure 5B, lanes 6–11), suggesting that I44 and V70 are mainly important for NEMO interaction in the first Ub. By contrast, residues L8 and H68 appear to be involved in the interaction of both Ub molecules with NEMO, as the L8A and H68A mutations on two Ub molecules reduced NEMO interaction more than the same mutations on either the first or the second Ub (lanes 3–5, 12–14). The L8A and H68A mutations in the first Ub reduced tandem di-Ub interaction with NEMO more than the same mutations in the second Ub, suggesting that L8 and H68 are somewhat more important for the interaction of the first Ub with NEMO. These data are very surprising and imply that the two Ub molecules in tandem di-Ub have significant differences in their interactions despite the dimeric symmetry of NEMO.

To determine whether the second Ub uses a different surface in NEMO interaction, we performed extensive mutagenesis that covered almost the entire surface of the tandem di-Ub (Figure 5C). Whereas most mutations had no observable effects in NEMO interactions, the T12D mutation of the second Ub had a selectively strong effect in NEMO binding (Figure 5B, lanes 30 and 31). Similarly, although the effects were less drastic, F4A and K6D mutations were partially defective when introduced in the second Ub but had no effect when introduced in the first Ub.

To investigate whether the C-terminal residues in either the first or the second Ub are important for NEMO interaction, we generated L73A and R74A mutations in either Ub molecule and a deletion of G75–G76 in the second Ub of the tandem di-Ub (Figure 5B, lanes 22–28). Both L73 and R74 appear to be involved in the first Ub interaction with NEMO, whereas the C-terminal residues of the second Ub contribute minimally to the interaction.

Mapping of L8, I44, H68, V70, L73, and R74 onto the surface of the first Ub (Figures 5D and 5E) and mapping of F4, K6, L8, T12, and H68 onto the surface of the second Ub (Figures 5E and 5F) both showed continuous NEMO-binding sites. The surface patch of the first Ub is centered at the conserved hydrophobic patch, while that of the second Ub is adjacent to and overlaps with the

(E) Mapping of mutational data of both the first and the second Ub onto the ribbon diagram of Ub. Red and pink, residues of the first Ub or both Ub molecules involved in NEMO interaction; cyan and light cyan, residues of the second Ub involved in NEMO interaction. The two ovals indicate approximate locations of the two NEMO-binding sites.

(F) Mapping of mutational data onto the second Ub surface of the tandem di-Ub. Cyan, drastic effects; light cyan, less drastic effects.

(G) Overlaid contour plots of the H^1 - N^{15} HSQC spectra of tandem di-Ub titrated with unlabeled NEMO at different molar ratios: 1:0 (free di-Ub, black), 1:0.1 (red), 1:0.15 (blue), 1:0.2 (green), 1:0.25 (purple), and 1:0.3 (cyan). Side-chain peaks are contained in the dashed box in the spectra.

(H) Mapping of residues that suffered severe intensity attenuation upon NEMO titration. Green, residues that appear to be selectively attenuated in one of the Ub molecules; blue, residues that appear to be attenuated in both Ub molecules. The ovals indicate the two potential separate NEMO-binding sites. S57 is right behind its labeled position. Residues not shown are buried.

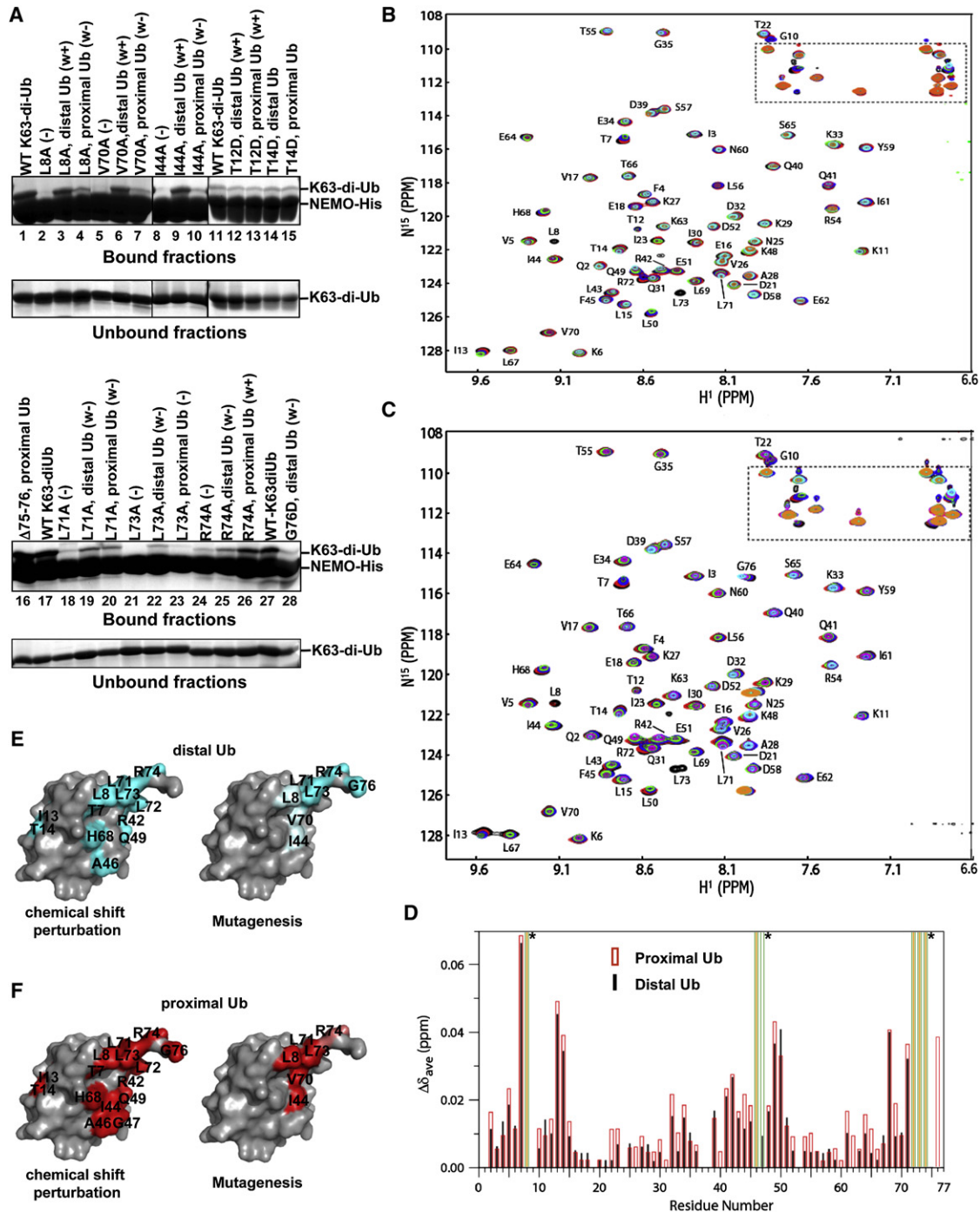


Figure 6. Structure-Based Mutagenesis and NMR Experiments on the NEMO:K63-Linked Di-Ub Interaction

(A) Mutations on K63-linked di-Ub. No effects, >0.8 of WT; w+, 0.5–0.8 of WT; w–, 0.2–0.5 of WT; –, <0.2 of WT.

(B) Overlaid contour plots of the H^1 - N^{15} HSQC spectra of K63-linked di-Ub selectively labeled at the distal Ub and titrated with unlabeled NEMO at different molar ratios: 1:0 (free di-Ub, black), 1:0.1 (red), 1:0.2 (blue), 1:0.3 (green), 1:0.4 (purple), 1:0.5 (cyan), and 1:0.75 (orange). Side-chain peaks are contained in the dashed box in the spectra.

(C) Overlaid contour plots of the H^1 - N^{15} HSQC spectra of K63-linked di-Ub selectively labeled at the proximal Ub and titrated with unlabeled NEMO at different molar ratios: 1:0 (free di-Ub, black), 1:0.1 (red), 1:0.2 (blue), 1:0.3 (green), 1:0.4 (purple), 1:0.5 (cyan), and 1:0.75 (orange). Side-chain peaks are contained in the dashed box in the spectra.

(D) Chemical shift perturbation ($\sqrt{(\Delta\delta^1H)^2 + (\Delta\delta^{15}N)^2/25}$) of distal (solid black bars) and proximal (open red bars) Ub residues upon titration with NEMO. Solid orange and open green bars near the asterisk indicate broadened peaks in distal and proximal Ub molecules, respectively.

hydrophobic patch identified for the first Ub (Figure 5E). Five of the six identified residues of the first Ub exhibited drastic effects when mutated. By contrast, only one of the five identified residues of the second Ub is critical for NEMO interaction, suggesting that the first Ub contributes more binding energy to the overall interaction of tandem di-Ub with NEMO.

To provide an independent assessment on the interaction of NEMO with tandem di-Ub, we used NMR titration experiments. The proton-nitrogen TROSY-HSQC spectrum of N^{15} -labeled tandem di-Ub is similar to published mono-Ub spectra (Wagner et al., 2008). However, a number of split resonances were observed, indicating subtle differences in the environment of these residues in the two Ub molecules. Titration of NEMO to tandem di-Ub in 0.05 intervals of molar ratio led to severe line broadening and associated intensity attenuation of selective resonances (Figures 5G and S3). The line broadening is characteristic of an intermediate exchange regime on the NMR time scale, which is generally consistent with the micromolar affinity of the NEMO:tandem di-Ub interaction. Significantly, among residues with split peaks, preferential disappearance of one of the peaks occurred for residues I3, T14, L15, L56, S57, K63, E64, and L73. This observation strongly supports that the NEMO interactions of the two Ub molecules are different. Among nonsplit peaks with severe intensity decay are residues T7, L8, I13, V70, and G75, suggesting that these residues are affected by NEMO interactions in both Ub molecules. When mapped onto the Ub surface, these residues cluster into two separate patches and cover the same side of the Ub molecule as identified from mutagenesis (Figure 5H).

The apparent involvement of Ub C-terminal regions in mutagenesis (L73 and R74) and NMR (L73) experiments prompted us to hypothesize that the linker between the two Ub molecules in tandem di-Ub may wrap around NEMO tightly. Indeed, deletion of a single residue G76 from the first Ub in tandem di-Ub completely abolished tandem di-Ub interaction with NEMO (Figure 5B, lane 33). We could not assess whether insertions of one or two Gly residues between the two Ub molecules affect interaction with NEMO because the insertion mutants were degraded to mono-Ub upon expression.

Mapping of Residues Important for NEMO Interaction with K63-Linked Di-Ub Using Mutagenesis and NMR Chemical Shift Perturbation

Given the similarity of surfaces that NEMO uses to recognize tandem and K63-linked di-Ub, we hypothesized that, vice versa, similar surfaces on Ub are used for NEMO interaction. To test this, we first generated eight mutants of K63-linked di-Ub, L8A, I44A, V70A, and T12D on the proximal Ub and the same on the distal Ub. T14D was also made on either of the Ub molecules as a control. The yields of di-Ub in the L8A, I44A, and V70A mutants were diminished by many fold, which is consistent with involvement of the conserved hydrophobic patch in both Ub charging

by E1 and Ub interaction with the E2 acceptor site at Uev1A. Pull-down of these mutants using the CC2-LZ of NEMO showed that L8A, I44A, and V70A mutations on the proximal Ub all led to impairment in NEMO interaction (Figure 6A, lanes 2–10). For the distal Ub, these mutations only had marginal effects. However, the L8A, I44A, and V70A double mutations of the K63-linked di-Ub diminished interaction with NEMO more severely than the same mutations on the proximal Ub alone. This suggests that L8, I44, and V70 are also involved in distal Ub interaction with NEMO, albeit with less energetic contribution (Figure 6A). T12D on either proximal or distal Ub had minimal effects in NEMO interaction. T14D had no effects in NEMO interaction.

Having established that the conserved hydrophobic patches of both proximal and distal Ub molecules are involved in NEMO interaction, we investigated whether the C-terminal regions of the Ub molecules also participate in this interaction. We generated L71A, L73A, and R74A mutations on both Ub, the G76D mutation on the distal Ub, and deletion of G75–G76 on the proximal Ub (Figure 6A, lanes 16–28). The G76D mutation of the distal Ub affected the efficiency of K63-linked di-Ub synthesis drastically, but we managed to obtain a sufficient amount for this study. Pull-down of K63-linked di-Ub mutants by His-tagged NEMO showed that residues L71, L73, R74, and G76 of the distal Ub are all critical in NEMO interaction. By contrast, for the proximal Ub, only the beginning part of the C-terminal tail is important; the involvement decreases at R74 and becomes minimal at the last two residues. The importance of G76 suggests that the K63 linkage per se may be recognized by NEMO.

To provide an independent assessment on the interaction between K63-linked di-Ub and NEMO, we performed NMR chemical shift perturbation experiments. We produced K63-linked di-Ub proteins that are selectively labeled with N^{15} either in the distal Ub or the proximal Ub, K63- N^{15} Ub_d-Ub_p, or K63-Ub_d- N^{15} Ub_p. The proton-nitrogen HSQC spectra of K63- N^{15} Ub_d-Ub_p and K63-Ub_d- N^{15} Ub_p are highly similar to each other and again to known mono-Ub HSQC spectra (Wagner et al., 2008). The resonance of residue K63 shifts in the spectrum of the proximal Ub-labeled construct, consistent with ligation of the distal Ub to this residue. Similarly, the C-terminal residue (G76) in the spectrum of distal Ub labeled construct is undetectable, consistent with its involvement in the isopeptide linkage to K63 of the proximal Ub. Titration of NEMO CC2-LZ domain into either of the N^{15} -labeled samples produced gradual chemical shift changes of resonances in the H^1 - N^{15} HSQC spectra with concomitant selective peak broadening and intensity reductions (Figures 6B and 6C). These spectral characteristics are consistent with an intermediate-fast exchange regime on the NMR time scale and in keeping with a lower affinity of the NEMO:K63-linked di-Ub interaction than the NEMO:tandem di-Ub interaction.

The patterns of chemical shift perturbation and peak broadening by NEMO were essentially identical for K63- N^{15} Ub_d-Ub_p

(E) Mapping of residues (cyan) with larger than 0.02 ppm chemical shift perturbation (left) and residues with mutational effects (right) onto the surface of distal Ub. For mutational effects, cyan indicates drastic effects and light cyan indicates weak effects. No residues are mapped to the reverse side of Ub.

(F) Mapping of residues (red) with larger than 0.02 ppm chemical shift perturbation (left) and residues with mutational effects (right) onto the surface of proximal Ub. For mutational effects, red indicates drastic effects and pink indicates weak effects. Only one residue D32 with significant chemical shift perturbation is mapped to the reverse side of Ub (not shown).

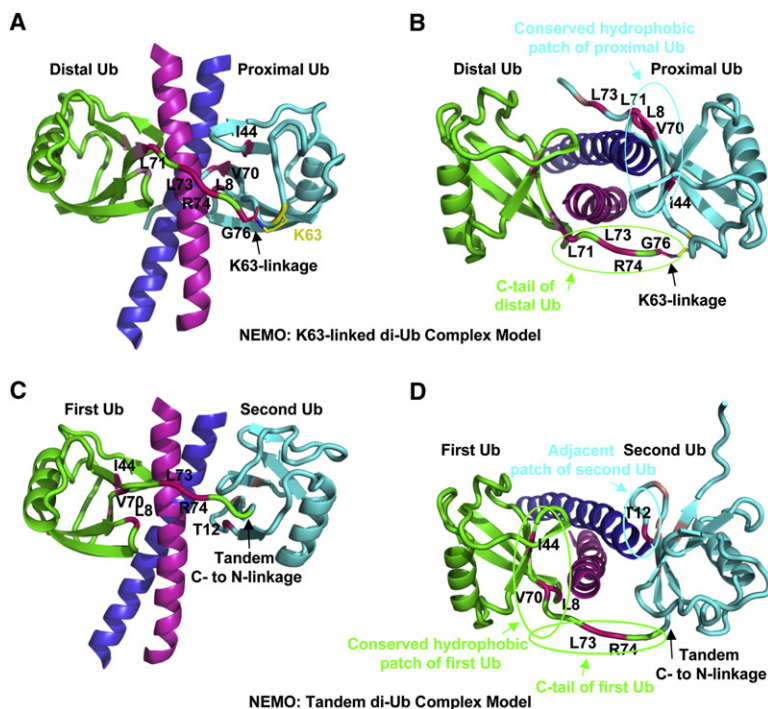


Figure 7. Model of NEMO:Di-Ub Interactions

(A) The NEMO:K63-linked di-Ub interaction model produced by HADDOCK. Only the LZ region of NEMO dimer is shown in blue and magenta for each chain, respectively. The distal and the proximal Ub molecules are in green and cyan, respectively. Residues critical for NEMO interaction are labeled and shown in red. Those that are less critical for NEMO interaction are shown in pink, but not labeled.

(B) Same as (A), but rotated approximately 90° around the horizontal axis. The critical interaction patches are circled by ovals. (C) The NEMO:tandem di-Ub interaction model produced by HADDOCK. Only the LZ region of NEMO dimer is shown in blue and magenta for each chain, respectively. The first and the second Ub molecules are in green and cyan, respectively. Residues critical for NEMO interaction are labeled and shown in red. Those that are less critical for NEMO interaction are shown in pink, but not labeled.

(D) Same as (C), but rotated approximately 90° around the horizontal axis. The critical interaction patches are circled by ovals.

and K63-Ub_d-N¹⁵Ub_p (Figure 6D). In both cases, residues with the largest chemical shift changes and severe peak broadening were clustered around L8, I44, and V70 shown by mutagenesis to be important for K63-linked di-Ub to interact with NEMO. Many C-terminal tail residues of both Ub molecules also exhibited significant chemical shift perturbation and peak broadening. Mapping of chemical shift changes larger than 0.02 ppm (0.02–0.07 ppm) and broadened residues in either the distal Ub (Figure 6E) or the proximal Ub (Figure 6F) to the surface of Ub showed that they agree very well with the mutagenesis data. They also reside on the same β sheet surface of Ub shown to be critical for tandem di-Ub interaction and at the C-terminal tails. These data, in conjunction with the mutagenesis data, strongly suggest that K63-linked di-Ub interacts with NEMO using similar, albeit not identical, surfaces. Unlike tandem di-Ub interaction with NEMO, the proximal and distal Ub molecules in K63-linked di-Ub use the same conserved surface patches for interacting with NEMO. However, based on the degree of mutational effects, the most important parts of K63-linked di-Ub for NEMO interaction are the proximal Ub and the C-terminal tail of the distal Ub. It is possible that the hydrophobic patch of the distal Ub does not contact NEMO as optimally as the proximal Ub.

Models of Interactions of NEMO with Tandem and K63-Linked Di-Ub

Our mutational data suggest that NEMO uses an essentially identical surface for tandem and K63-linked di-Ub interaction. By contrast, the mutational and NMR data on the interaction of NEMO with its tandem and K63-linked di-Ub binding partners mapped similar, but not identical surfaces on the Ub molecules. On the β sheet face of Ub, there are two patches that Ub uses for NEMO interaction. The first patch is composed of the conserved

hydrophobic surface of Ub, which is used for both molecules of the K63-linked di-Ub and for the first Ub of the tandem di-Ub in NEMO interaction. The second patch is adjacent to and overlaps with the first patch on the same side of the β sheet of Ub and is used for the second Ub of tandem di-Ub in NEMO interaction. Because of the intrinsic flexibility of the C-terminal tail, we did not use its experimental data in creating models of NEMO:di-Ub interactions.

We employed the high-ambiguity-driven protein-protein docking program HADDOCK (Dominguez et al., 2003) to generate the two types of NEMO:Ub complexes using the mutational and NMR data as restraints. For both types of interactions, we entered NEMO residues that reduced di-Ub interaction when mutated as “active residues” directly involved in the interaction. Those that did not cause observable effects in di-Ub interaction when mutated were entered as “passive residues.” To generate the first type of NEMO:Ub interaction, we did three different runs with (1) L8, I44, H68, and V70, residues implicated from mutagenesis as “active residues”; (2) proximal Ub residues that had undergone significant chemical shift perturbation during NEMO titration as “active residues”; and (3) distal Ub residues that had undergone significant chemical shift perturbation during NEMO titration as “active residues.” All three runs gave the same cluster of low-energy complexes.

To build the NEMO:K63-linked di-Ub complex, we generated the symmetry mate of the docked Ub that interacts with the other side of the NEMO dimer. This produced two symmetrical interactions with experimentally identified important residues of NEMO and Ub facing each other. Slight modifications to the conformations of the C-terminal tail (residues 71–76) of the distal Ub and the K63 side chain of the proximal Ub were needed to generate a geometrically correct K63 linkage (Figure 7A). In this model, the C-terminal tail of distal Ub wraps around NEMO, consistent with the mutagenesis data on the importance of this region. We also built the C-terminal tail of the proximal Ub so that its beginning part contacted NEMO. Inspection of the location of the N terminus of the proximal Ub in this complex shows that it is

12 Å away from the C-terminal carboxylate of the distal Ub. This suggests that it is not possible for tandem di-Ub to interact with NEMO in the same fashion.

To generate the second type of interface for building the NEMO:tandem di-Ub complex, we used residues F4, K6, L8, T12, and H68, which were implicated by mutagenesis in the interaction of the second Ub with NEMO as “active residues” in the docking run. We placed the low-energy cluster of the docked second type complex with the first type complex as the starting point for the asymmetrical complex in the NEMO:tandem di-Ub interaction. Residue T12, which was identified as the most critical for the second type of interaction, resides at the center of this interface. Rebuilding of the C-terminal tail of the first Ub easily connected it to the N terminus of the second Ub (Figure 7B).

A key feature of both NEMO:tandem di-Ub and NEMO:K63-linked di-Ub models is that the di-Ub stretches both its Ub molecules to clasp around NEMO, like a hand gripping on a rope in a U-shaped fashion. The major Ub-contacting sites of NEMO in both complexes are at the center of the surface patch identified from mutagenesis. In addition, the regions at or near the tandem and the K63 linkages are contacting NEMO. The modeling of NEMO:tandem di-Ub and NEMO:K63-linked di-Ub complexes provided an integral understanding of the similarity and differences in the recognition of tandem and K63-linked di-Ub by NEMO.

DISCUSSION

The transcription factor NF-κB regulates expression of numerous genes controlling immune and stress responses, inflammatory reaction, and protection against apoptosis (Gilmore, 2006). NF-κB may be activated in many signaling pathways, including the TNF receptor superfamily, IL-1 receptor/Toll-like receptor superfamily, the T cell receptor, and the B cell receptor (Scheiderer, 2006). While the upstream adaptors in these pathways may be different, they all induce K63-linked polyubiquitination. By interacting with K63-linked poly-Ub, NEMO integrates the diverse receptor activation signals to IKK signalosome recruitment and activation.

Our current studies provide a mechanistic basis for the interaction of NEMO with di-Ub. Unlike known helical motifs in Ub interaction, dimeric NEMO possesses composite binding sites from both of its chains for interacting with tandem and K63-linked di-Ub. Certain degrees of asymmetry in binding energy and geometry are present in both tandem and K63-linked di-Ub interactions with NEMO. For tandem di-Ub, the first Ub uses its conserved hydrophobic patch, while the second Ub uses an adjacent patch. While the C-terminal tail of the first Ub is important, the C-terminal tail of the second Ub does not seem to be involved at all in the interaction, as it points away from NEMO. The mutational effects suggest that the first Ub contributes many more critical residues (L8, I44, V70, L73, and R74) than the second Ub (T12) and is energetically dominant. For K63-linked di-Ub, the proximal Ub appears to have an optimal interaction at its conserved hydrophobic patch (L8, I44, V70, L71, and L73). A major contribution of the distal Ub is its C-terminal tail (L71, L73, R74, and G76); by contrast,

its hydrophobic patch contributes much less to the NEMO interaction.

While most known Ub-binding domains recognize mono-Ub, the UBA domains seem to interact with either mono-Ub or di-Ub (Hurley et al., 2006; Varadan et al., 2005). UBA domains are compact three-helical bundles. In the NMR-derived model of the hHR23A UBA2 domain in complex with K48-linked di-Ub, the two Ub molecules grip onto either side of the UBA domain (Varadan et al., 2005), reminiscent of our proposed modes of di-Ub interactions with NEMO. Although K63-linked di-Ub in principle could also grip onto UBA2 in manner similar to K48-linked di-Ub, it binds to UBA2 in a mono-Ub-like mode with much less affinity. This difference was attributed to the additional energetic loss from immobilizing a second Ub in a K63-linked di-Ub because K63-linked chains possess few inter-Ub contacts (Varadan et al., 2005). By contrast, the K48-linked chain adopts a closed conformation with stable inter-Ub contacts in which the individual Ub molecules are already immobilized relative to each other (Cook et al., 1994).

An intrinsic conformational difference may also explain the affinity differential between tandem and K63-linked di-Ub. There are many split peaks in the NMR spectrum of tandem di-Ub, suggesting the presence of inter-Ub interactions. By contrast, and in agreement with previous data, the NMR spectra of K63-linked di-Ub samples that were selectively labeled either at the proximal or the distal Ub were almost identical. Therefore, tandem di-Ub may experience less energetic cost for immobilizing both Ub molecules upon NEMO interaction in comparison with the NEMO:K63-linked di-Ub interaction. Consistent with this assessment, the distal Ub in K63-linked di-Ub appears to contribute less to the overall interaction. Another factor in the lower affinity of the NEMO:K63-linked di-Ub interaction may be due to a “suboptimal” contact of the distal Ub hydrophobic patch with NEMO; although our model of the complex has the same mode of interaction at this site, we cannot exclude the possibility of subtle differences. It has been shown that longer K63-linked chains are more efficient in NEMO interaction, which is likely a result of further NEMO oligomerization and avidity (Wu et al., 2006). The weakest interaction of K48-linked di-Ub with NEMO may be due to the different geometric relationship of the two Ub molecules imposed by the K48 linkage. The consequence may be that the two Ub molecules cannot reach the equivalent Ub-binding sites of NEMO simultaneously or that the isopeptide linkage region does not have an optimal interaction with NEMO. However, it is possible that a K48-linked di-Ub also has some additional favorable contacts so that it interacts with NEMO better than a mono-Ub.

The robust affinity of NEMO to the natural Ub precursors such as tandem di-Ub raises the question whether this interaction may be relevant in vivo at certain physiological settings. In this regard, the most recent report showed that an E3 complex known as LUBAC interacts with NEMO, conjugates tandem polyubiquitin chains to NEMO, and activates the canonical NF-κB pathway (Tokunaga et al., 2009).

Recently, the crystal structures of K63-linked di-Ub in complex with the deubiquitinating enzyme AMSH-LP (Sato et al., 2008) and with the Fab fragment of the specific antibody

raised to recognize K63-linked chains (Newton et al., 2008) have been reported. Although the K63-linked di-Ub structures in both complexes are extended with little inter-Ub contact, they cannot be superimposed due to the complete difference in the spatial relationships of the proximal and distal Ub. Furthermore, the Ub surfaces used in complex formation are also distinct. While the distal Ub uses the hydrophobic patch for interaction with AMSH-LP, it is only peripherally involved in the Fab interaction. Neither of the hydrophobic patches of the proximal Ub is central to the recognitions. The conformation of K63-linked di-Ub in NEMO interaction is again completely different from either of the complexes above, and the hydrophobic patches of both proximal and distal Ub are engaged in NEMO interaction. It appears then that nature has developed a diverse repertoire of interactions to provide specificity of Ub recognition in biological processes.

EXPERIMENTAL PROCEDURES

Protein Expression, Purification, Crystallization, and Structure Determination

NEMO and Ub were expressed in *E. coli* and purified by ion exchange and gel filtration chromatography. NEMO CC2-LZ (residues 246–337) were crystallized under 10% PEG1 K and 10% PEG4 K in Tris-HCl at pH 8.0. The structure was solved by single-wavelength anomalous diffraction. Mono-Ub mutants K63R-Ub and D77-Ub were generated for enzymatic synthesis of K63-linked di-Ub according to the published protocol (Piotrowski et al., 1997). For NMR experiments, the K63R-Ub and the D77-Ub mutants were expressed in minimal media supplemented with $N^{15}H_4Cl$.

NMR Spectroscopy

Samples for NMR experiments were made to a final protein concentration of 400 μM in the case of N^{15} -labeled tandem di-Ub or 200 μM for K63-linked di-Ub with either the distal or the proximal Ub N^{15} labeled. NMR experiments were performed on a 600 MHz Varian INOVA equipped with a cryogenic probe, at a sample temperature of 25°C. Spectra were recorded in succession starting with the collection of the control spectra (di-Ub alone) and by adding the corresponding molar ratio of NEMO in 0.05 molar increments.

Stable NEMO-Expressing Cell Lines

NEMO-deficient MEFs stably expressing wild-type NEMO have been described (Wu et al., 2006), and NEMO-deficient MEFs stably reconstituted with the E315A mutant of NEMO were generated by the same method.

ACCESSION NUMBERS

The coordinates have been deposited in the RCSB Protein Data Bank with the PDB code of 3FX0.

SUPPLEMENTAL DATA

The Supplemental Data include Supplemental Experimental Procedures and three figures and can be found with this article online at [http://www.cell.com/molecular-cell/supplemental/S1097-2765\(09\)00039-2](http://www.cell.com/molecular-cell/supplemental/S1097-2765(09)00039-2).

ACKNOWLEDGMENTS

We thank Drs. Narayanasami Sukumar, Kanagalaghatta Rajashankar, and Igor Kourinov for data collection at NE-CAT of APS; Prof. Dinshaw Patel for use of the Micro Calorimetry System instrument; Dr. Haitao Li for help with the ITC experiments; Dr. Xuejun Jiang for providing E1 for enzymatic synthesis of K63-linked di-Ub; and Jin Wu for maintaining X-ray equipment and computers. Y.-C.L. and S.-C. L. are postdoctoral fellows of the Cancer Research Institute.

Received: October 18, 2008

Revised: January 12, 2009

Accepted: January 20, 2009

Published online: January 29, 2009

REFERENCES

- Agou, F., Ye, F., Goffinont, S., Courtois, G., Yamaoka, S., Israel, A., and Veron, M. (2002). NEMO trimerizes through its coiled-coil C-terminal domain. *J. Biol. Chem.* 277, 17464–17475.
- Chen, Z.J. (2005). Ubiquitin signalling in the NF-kappaB pathway. *Nat. Cell Biol.* 7, 758–765.
- Cook, W.J., Jeffrey, L.C., Kasperek, E., and Pickart, C.M. (1994). Structure of tetraubiquitin shows how multiubiquitin chains can be formed. *J. Mol. Biol.* 236, 601–609.
- Courtois, G., and Gilmore, T.D. (2006). Mutations in the NF-kappaB signaling pathway: implications for human disease. *Oncogene* 25, 6831–6843.
- Dominguez, C., Boelens, R., and Bonvin, A.M. (2003). HADDOCK: a protein-protein docking approach based on biochemical or biophysical information. *J. Am. Chem. Soc.* 125, 1731–1737.
- Ea, C.K., Deng, L., Xia, Z.P., Pineda, G., and Chen, Z.J. (2006). Activation of IKK by TNFalpha requires site-specific ubiquitination of RIP1 and polyubiquitin binding by NEMO. *Mol. Cell* 22, 245–257.
- Filipe-Santos, O., Bustamante, J., Haverkamp, M.H., Vinolo, E., Ku, C.L., Puel, A., Frucht, D.M., Christel, K., von Bernuth, H., Jouanguy, E., et al. (2006). X-linked susceptibility to mycobacteria is caused by mutations in NEMO impairing CD40-dependent IL-12 production. *J. Exp. Med.* 203, 1745–1759.
- Gilmore, T.D. (2006). Introduction to NF-kappaB: players, pathways, perspectives. *Oncogene* 25, 6680–6684.
- Herscovitch, M., Comb, W., Ennis, T., Coleman, K., Yong, S., Armstead, B., Kalaitzidis, D., Chandani, S., and Gilmore, T.D. (2008). Intermolecular disulfide bond formation in the NEMO dimer requires Cys54 and Cys347. *Biochem. Biophys. Res. Commun.* 367, 103–108.
- Hurley, J.H., Lee, S., and Prag, G. (2006). Ubiquitin-binding domains. *Biochem. J.* 399, 361–372.
- Newton, K., Matsumoto, M.L., Wertz, I.E., Kirkpatrick, D.S., Lill, J.R., Tan, J., Dugger, D., Gordon, N., Sidhu, S.S., Fellouse, F.A., et al. (2008). Ubiquitin chain editing revealed by polyubiquitin linkage-specific antibodies. *Cell* 134, 668–678.
- Oeckinghaus, A., Wegener, E., Welteke, V., Ferch, U., Arslan, S.C., Ruland, J., Scheidereit, C., and Krappmann, D. (2007). Malt1 ubiquitination triggers NF-kappaB signaling upon T-cell activation. *EMBO J.* 26, 4634–4645.
- Piotrowski, J., Beal, R., Hoffman, L., Wilkinson, K.D., Cohen, R.E., and Pickart, C.M. (1997). Inhibition of the 26 S proteasome by polyubiquitin chains synthesized to have defined lengths. *J. Biol. Chem.* 272, 23712–23721.
- Sato, Y., Yoshikawa, A., Yamagata, A., Mimura, H., Yamashita, M., Ookata, K., Nureki, O., Iwai, K., Komada, M., and Fukai, S. (2008). Structural basis for specific cleavage of Lys 63-linked polyubiquitin chains. *Nature* 455, 358–362.
- Scheidereit, C. (2006). I kappa B kinase complexes: gateways to NF-kappaB activation and transcription. *Oncogene* 25, 6685–6705.
- Sebban-Benin, H., Pescatore, A., Fusco, F., Pascuale, V., Gautheron, J., Yamaoka, S., Moncla, A., Ursini, M.V., and Courtois, G. (2007). Identification of TRAF6-dependent NEMO polyubiquitination sites through analysis of a new NEMO mutation causing incontinentia pigmenti. *Hum. Mol. Genet.* 16, 2805–2815.
- Tokunaga, F., Sakata, S.I., Saeki, Y., Satomi, Y., Kirisako, T., Kamei, K., Nakagawa, T., Kato, M., Murata, S., Yamaoka, S., et al. (2009). Involvement of linear polyubiquitylation of NEMO in NF-kappaB activation. *Nat. Cell Biol.* Published online January 11, 2009. 10.1038/ncb1821.
- Varadan, R., Assfalg, M., Raasi, S., Pickart, C., and Fushman, D. (2005). Structural determinants for selective recognition of a Lys48-linked polyubiquitin chain by a UBA domain. *Mol. Cell* 18, 687–698.
- Vinolo, E., Sebban, H., Chaffotte, A., Israel, A., Courtois, G., Veron, M., and Agou, F. (2006). A point mutation in NEMO associated with anhidrotic

ectodermal dysplasia with immunodeficiency pathology results in destabilization of the oligomer and reduces lipopolysaccharide- and tumor necrosis factor-mediated NF-kappa B activation. *J. Biol. Chem.* 281, 6334–6348.

Wagner, S., Carpentier, I., Rogov, V., Kreike, M., Ikeda, F., Lohr, F., Wu, C.J., Ashwell, J.D., Dotsch, V., Dikic, I., et al. (2008). Ubiquitin binding mediates the NF-kappaB inhibitory potential of ABIN proteins. *Oncogene* 27, 3739–3745.

Wu, C.J., Conze, D.B., Li, T., Srinivasula, S.M., and Ashwell, J.D. (2006). Sensing of Lys 63-linked polyubiquitination by NEMO is a key event in NF-kappaB activation. *Nat. Cell Biol.* 8, 398–406.

Wu, C.J., and Ashwell, J.D. (2008). NEMO recognition of ubiquitinated Bcl10 is required for T cell receptor-mediated NF-kappaB activation. *Proc. Natl. Acad. Sci. USA* 105, 3023–3028.

Supplemental Data

Structural Basis for Recognition

of Diubiquitins by NEMO

Yu-Chih Lo, Su-Chang Lin, Carla C. Rospigliosi, Dietrich B. Conze, Chuan-Jin Wu, Jonathan D. Ashwell, David Eliezer, and Hao Wu

Supplemental Experimental Procedures

Cloning, Protein Expression and Purification

NEMO and Ub cDNA fragments were cloned into the pET28a or pET26b expression vectors (Novagen) with or without hexahistidine tags (His-tags). Tandem di-Ub was generated by ligating two Ub genes and the restriction site between the two genes was deleted by the procedures implemented in the protocol of QuikChange site-directed mutagenesis kit (Stratagene). Mutagenesis of NEMO and di-Ub was also performed according to the QuikChange protocol. After transformation with the plasmids, *E. coli* BL21(DE3) RIPL cells were grown in Luria broth supplemented with 35 µg/mL kanamycin at 37 °C to an A_{600} of 1.0. Protein expression was induced by adding 0.5 mM isopropyl thio-β-D-galactopyranoside (IPTG), and the cells were grown overnight at 20 °C. Cells were pelleted by centrifugation at 5,000 rpm and resuspended in buffer A containing 50 mM sodium phosphate at pH 7.5, 300 mM NaCl, 5 mM β-mercaptoethanol and 20 mM imidazole. The cells were lysed by sonication, and the lysate was centrifuged at 16,000 rpm for 45 min. For purification of proteins with His-tags, the supernatant was incubated with Ni-NTA beads (Qiagen) for 2 hr at 4 °C. The beads were loaded onto a column and washed with buffer B containing 50 mM sodium phosphate at pH 7.5, 300 mM NaCl, 5 mM β-mercaptoethanol and 40 mM imidazole. The protein was eluted with buffer C containing 50 mM sodium phosphate at pH 7.5, 300 mM NaCl, 5 mM β-mercaptoethanol, and 500 mM imidazole. For sample preparation for crystallization, affinity-purified NEMO was further subjected to gel filtration chromatography using Superdex 200 10/300 GL (GE Healthcare), which was pre-equilibrated with a solution of 20 mM Tris-HCl at pH 8.0 and 150 mM NaCl.

His-tagged NEMO Pull-down Assay

WT and mutant His-tagged NEMO proteins were first purified with Ni-NTA beads and their expression levels were assessed by SDS-PAGE. Beads containing estimated equivalent quantities of NEMO proteins were mixed with the cell lysate of non-tagged WT or mutant tandem di-Ub, or WT or mutant K63-linked di-Ub in the presence of buffer A. The mixtures were incubated at room temperature for 1.5 hours with rotation. After centrifugation, the supernatants were removed and subject to SDS-PAGE analysis (unbound fractions). The beads were then washed twice with buffer B and subject to SDS-PAGE analysis (bound fractions). All pull-down experiments were repeated two to four times with consistency. For di-Ub mutants, the pull-down gels were quantified with the KODAK 1D Image Analysis Software and normalized against the WT di-Ub. No effects: >0.8 of WT; w+: 0.5-0.8 of WT; w-: 0.2-0.5 of WT; -: <0.2 of WT.

Multi-angle Light Scattering (MALS) Analyses

The molar masses of NEMO and the NEMO-Ub complexes were determined by MALS. Protein sample was injected into a Superdex 200 (10/300 GL) gel filtration column (GE Healthcare) equilibrated in a buffer containing 20 mM Tris at pH 8.0 and 150 mM NaCl. The chromatography system was coupled to a three-angle light scattering detector (mini-DAWN TRISTAR) and a refractive index detector (Optilab DSP) (Wyatt Technology). Data were collected every 0.5 s with a flow rate of 0.2 mL/min. Data analysis was carried out using ASTRA V.

Isothermal Titration Calorimetry (ITC) and Data Analysis

Prior to analysis, purified His-tagged NEMO (residues 251-350), tandem di-Ub, or K63-linked di-Ub were subjected to gel filtration using the Superdex 200 HR10/30 column (GE Healthcare) in phosphate buffered saline (PBS). ITC measurements were performed at 25°C using iTC200 that was connected to a computer with ORIGIN software (Microcal Inc, Northampton, MA). Prior to titration, the protein samples were centrifuged at 10,000 rpm at 4 °C for 10 min to remove any debris and degassed by vacuum aspiration for ~10 min. The calorimeter cell and titration syringe were extensively rinsed with PBS. For the NEMO: tandem di-Ub interaction, the calorimetric titration was carried out at 25 °C with 32 injections of 1.25 µl 1.34 mM NEMO, spaced 120 s apart, into the sample cell containing a solution of 200 µl 56 µM di-Ub. Similarly, 2.2 mM NEMO was titrated into the sample cell containing 200 µl of 80 µM K63-linked di-Ub in 1 injection of 0.4 µl and 23 injections of 1.6 µl each. Each NEMO protein was also titrated into the sample cell of buffer alone to obtain the heat of dilution. After subtracting the heat of dilution, the association constant (K_A), enthalpy change (ΔH) and the stoichiometry (N) were obtained by fitting the thermograms to a single binding site model using the ORIGIN software. The remaining thermodynamic parameters, the dissociation constant (K_D), free energy change (ΔG), and the entropy change (ΔS) were calculated from the relationships:

$$K_A^{-1} = K_D \text{ and } -RT \ln K_A = \Delta G = \Delta H - T \Delta S$$

Crystallization and Structure Determination

Selenomethionine-substituted WT and L267M mutant proteins of NEMO CC2-LZ (residues 246-337) were crystallized at 4 °C with the hanging drop vapor diffusion method under 10% PEG1K and 10% PEG4K in Tris-HCl at pH 8.0. Single-wavelength anomalous diffraction data sets were collected at the NE-CAT beam line at the Advanced Photon Source. Diffraction data were processed and scaled using the HKL2000 software (Otwinowski and Minor, 1997). The crystals belong to space group $P6_5$. Selenium sites and phases were determined with direct method calculations in HKL2MAP (Pape and Schneider, 2004). Facilitated by the known selenium sites as markers for methionine residues, two molecules in the crystallographic asymmetric unit were traced and built (residues 263–333 for one chain and residues 267-329 for the other chain) using Coot (Emsley and Cowtan, 2004). All crystallographic refinement calculations were performed in CNS (Brunger et al., 1998), and the structures were displayed with PyMOL (DeLano Scientific).

Enzymatic Synthesis and Purification of K63-linked di-Ub

Mono-Ub mutants K63R-Ub and D77-Ub were generated for enzymatic synthesis of K63-linked di-Ub (Piotrowski et al., 1997). They were expressed in *E. coli* and purified using perchloric acid precipitation and cation exchange as described previously (Hofmann and Pickart, 2001). To synthesize WT K63-linked di-Ub, 0.5 mM K63R-Ub and 0.5 mM D77-Ub were mixed with 0.15

μM of E1, 8 μM of the E2 complex Ubc13/Uev1A, 5 mM ATP, and 0.5 mM DTT at 37°C overnight. Di-Ub was first purified from un-reacted mono-Ub and the enzymes using cation exchange. This is then followed by gel filtration chromatography for further purification and buffer exchange. For NMR experiments, the K63R-Ub and the D77-Ub mutants were expressed in minimal media supplemented with $\text{N}^{15}\text{H}_4\text{Cl}$. These mono-Ub mutants were then used for di-Ub synthesis as described for WT di-Ub. Potential NEMO-binding mutations were introduced on either the K63R-Ub or the D77-Ub for generation of specific mutations on either the proximal or the distal Ub in K63-linked di-Ub. Because some of the Ub mutations affected the efficiency of the ubiquitination reactions, the concentrations of the mono-Ub variants were adjusted to obtain sufficient amounts of purified di-Ub for pull-down experiments.

Nuclear Magnetic Resonance (NMR) Spectroscopy

Samples for NMR experiments were made to a final protein concentration of 400 μM in the case of N^{15} -labeled tandem di-Ub or 200 μM for K63-linked di-Ub with either the distal or the proximal Ub N^{15} -labeled. All protein solutions contained 100 mM NaCl, 10 mM Na_2HPO_4 , pH 7.4 (PBS) in 90 %/10 % $\text{H}_2\text{O}/\text{D}_2\text{O}$. NMR experiments were performed on a 600 MHz Varian INOVA equipped with a cryogenic probe, at a sample temperature of 25 °C. Spectra were recorded in succession starting with the collection of the control spectra (di-Ub alone) and by adding the corresponding molar ratio of NEMO in 0.05 molar increments. All NMR data were processed with NMRPipe (Delaglio et al., 1995) and analyzed using NMRView (Johnson and Blevins, 1994). Spectra were referenced indirectly to DSS and ammonia (Wishart et al., 1995) using the known chemical shift of water. Resonance assignments were based on previously reported assignments. For tandem di-Ub, most split peaks could be assigned unambiguously, but a few peaks (Q2, V17, E18) exhibited larger splittings which led to tentative assignments.

Stable NEMO-expressing Cell Lines

NEMO-deficient murine embryonic fibroblasts (MEFs) were provided by M. Schmidt-Supprian (Harvard University, Boston, MA). NEMO-deficient MEFs stably expressing wild-type NEMO have been described (Wu et al., 2006), and NEMO-deficient MEFs stably reconstituted with the E315A mutant of NEMO were generated by the same method. Briefly, Phoenix-Ampho cells were transfected with pMSCVpuro encoding HA-NEMO-E315A using Lipofectamine 2000 (Invitrogen). The retrovirus was collected and used to infect NEMO-deficient MEFs. Following selection with puromycin for 7 days, clones were isolated, expanded and analyzed for NEMO expression by immunoblotting. Clones expressing mutant NEMO levels comparable to those of clones reconstituted with wild-type NEMO were selected for experiments.

GST-NEMO Pull-downs of Polyubiquitinated IRAK-1

pGEX4T1-NEMO have been described (Wu et al., 2006). GST and GST-fusion proteins were expressed in *E. coli* and purified from the bacterial lysates using glutathione-Sepharose-4B beads (GE Healthcare). For NEMO binding to polyubiquitinated IRAK-1, lysates from 293 cells stably expressing IL-1R (293/IL-1R/TLR4/MD2) (Qin et al., 2005) were incubated with GST proteins for 16 hr at 4°C. The bead-bound complexes were extensively washed with lysis buffer, eluted with sample buffer, resolved by SDS-PAGE, and immunoblotted with anti-IRAK-1.

Immunoblotting

Cells were lysed in lysis buffer containing 20 mM Tris pH7.5, 150 mM NaCl, 1 % Triton X-100, 1 mM EDTA, 30 mM NaF, 2 mM sodium pyrophosphate supplemented with protease inhibitor

cocktail (Roche) and 1 mM N-ethylmaleimide. Lysates were normalized to protein concentration, denatured in sample buffer, resolved by SDS-PAGE, and immunoblotted with the indicated antibodies. Antibodies to I κ B (C-21), ubiquitin (P4D1), NEMO (FL-419), and IRAK-1 (F-4) were purchased from Santa Cruz Biotechnology. Immunoblots were visualized using horseradish peroxidase-conjugated secondary antibodies and enhanced chemiluminescence (Pierce).

Supplemental References

Brunger, A.T., Adams, P.D., Clore, G.M., DeLano, W.L., Gros, P., Grosse-Kunstleve, R.W., Jiang, J.S., Kuszewski, J., Nilges, M., Pannu, N.S., *et al.* (1998). Crystallography & NMR system: A new software suite for macromolecular structure determination. *Acta Crystallogr D54*, 905-921.

Delaglio, F., Grzesiek, S., Vuister, G.W., Zhu, G., Pfeifer, J., and Bax, A. (1995). NMRPipe: a multidimensional spectral processing system based on UNIX pipes. *J Biomol NMR* 6, 277-293.

Emsley, P., and Cowtan, K. (2004). Coot: model-building tools for molecular graphics. *Acta Crystallogr D Biol Crystallogr* 60, 2126-2132.

Hofmann, R.M., and Pickart, C.M. (2001). In vitro assembly and recognition of Lys-63 polyubiquitin chains. *J Biol Chem* 276, 27936-27943.

Johnson, B.A., and Blevins, R.A. (1994). A computer program for the visualization and analysis of NMR data. *Journal of Biomolecular NMR* 4, 603-614.

Otwinowski, Z., and Minor, W. (1997). Processing of X-ray diffraction data collected in oscillation mode. *Methods Enzymol* 276, 307-326.

Pape, T., and Schneider, T.R. (2004). HKL2MAP: a graphical user interface for phasing with SHELX programs. *J Appl Cryst* 37, 843-844.

Piotrowski, J., Beal, R., Hoffman, L., Wilkinson, K.D., Cohen, R.E., and Pickart, C.M. (1997). Inhibition of the 26 S proteasome by polyubiquitin chains synthesized to have defined lengths. *J Biol Chem* 272, 23712-23721.

Qin, J., Qian, Y., Yao, J., Grace, C., and Li, X. (2005). SIGIRR inhibits interleukin-1 receptor- and toll-like receptor 4-mediated signaling through different mechanisms. *J Biol Chem* 280, 25233-25241.

Wishart, D.S., Bigam, C.G., Yao, J., Abildgaard, F., Dyson, H.J., Oldfield, E., Markley, J.L., and Sykes, B.D. (1995). ¹H, ¹³C and ¹⁵N chemical shift referencing in biomolecular NMR. *J Biomol NMR* 6, 135-140.

Wu, C.J., Conze, D.B., Li, T., Srinivasula, S.M., and Ashwell, J.D. (2006). Sensing of Lys 63-linked polyubiquitination by NEMO is a key event in NF-kappaB activation [corrected]. *Nat Cell Biol* 8, 398-406.

Figure S1. Mutational effects of NEMO in interaction with commercial K63-linked di-Ub (Boston Biochem)

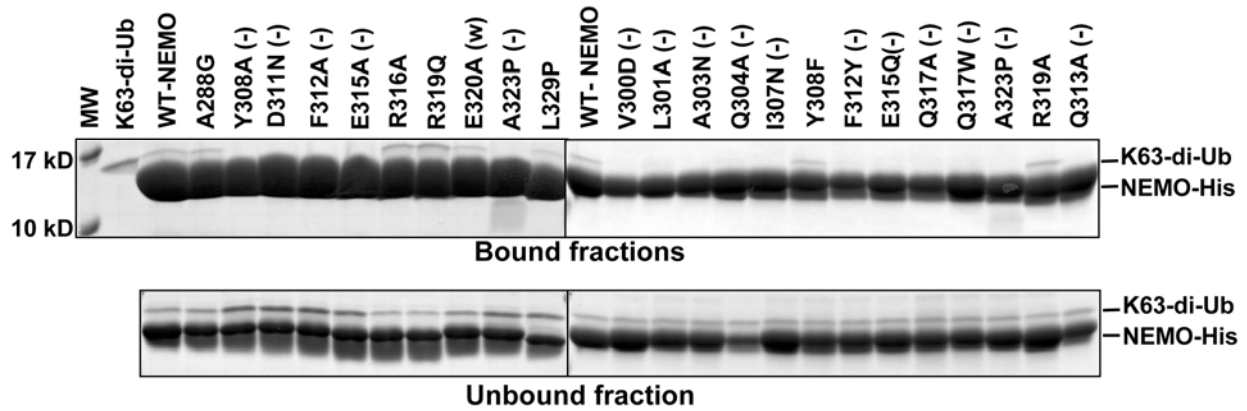


Figure S2. Multi-angle light scattering (MALS) measurements on additional NEMO mutants

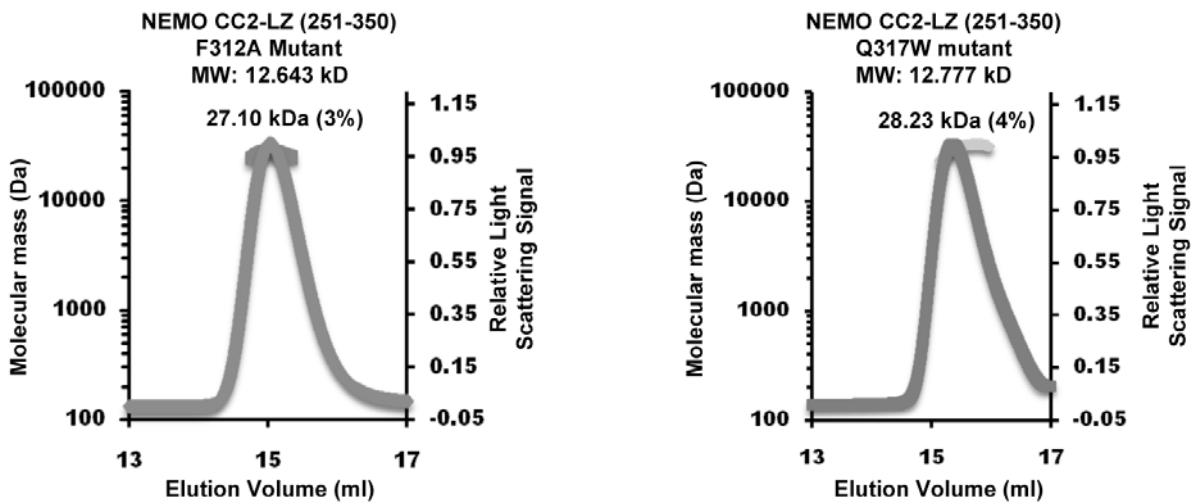


Figure S3. Overlaid histograms showing the intensity ratio for the peaks that are well-resolved in the ^1H - ^{15}N TROSY-HSQC spectra of tandem di-Ub upon titration of unlabeled NEMO at a 1:0.15 molar ratio. Orange filled bars and red empty bars represent the intensity ratio for each of the split peaks. For non-split peaks, orange filled bars and red empty bars are the same. Resonances for Q2, V17, and E18 exhibited large splittings which led to tentative assignments and were not used in interpretation of the interaction.

